Journal of Colloid and Interface Science 660 (2024) 896–906

Contents lists available at ScienceDirect

Journal of Colloid And Interface Science

journal homepage: www.elsevier.com/locate/jcis

Regular Article

Enhanced solubility of methyl ester sulfonates below their Krafft points in mixed micellar solutions

Veronika I. Yavrukova [a], Krassimir D. Danov [a,*], Tatiana G. Slavova [a], Rumyana D. Stanimirova [a], Yee Wei Ung [b], Alvin Tong Kim Suan [b], Hui Xu [b], Jordan T. Petkov [a,c]

[a] Department of Chemical & Pharmaceutical Engineering, Faculty of Chemistry & Pharmacy, Sofia University, Sofia 1164, Bulgaria
[b] KLK OLEO, KL-Kepong Oleomas Sdn Bhd, Menara KLK, Jalan PJU 7/6, Mutiara Damansara, Petaling Jaya, Selangor Dalur Ehsan 47810, Malaysia
[c] Biological Physics, School of Physics and Astronomy, The University of Manchester, Schuster Building, Oxford Road, M13 9PL, UK

GRAPHICAL ABSTRACT

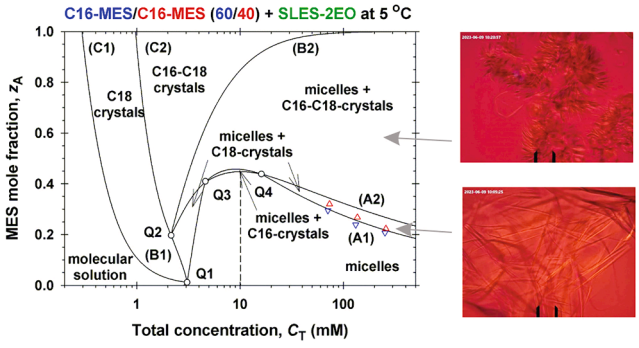

ARTICLE INFO

Keywords:
Methyl esters sulfonates (MES)
Sodium alpha olefin sulfonate (AOS)
Sodium lauryl ether sulfate with two ethylene oxide groups (SLES-2EO)
Ionic surfactant mixtures – phase diagrams
Micelle–crystallite coexistence

ABSTRACT

Hypothesis: Methyl ester sulfonates (MES) show limited water solubility at lower temperatures (Krafft point). One way to increase their solubility below their Krafft points is to incorporate them in anionic surfactant micelles. The electrostatic interactions between the ionic surfactant molecules and charged micelles play an important role for the degree of MES solubility.

Experiments: The solubility and electrolytic conductivity for binary and ternary surfactant mixtures of MES with anionic sodium alpha olefin sulfonate (AOS) and sodium lauryl ether sulfate with two ethylene oxide groups (SLES-2EO) at 5 °C during long-term storage were measured. Phase diagrams were established; a general phase separation theoretical model for their explanation was developed and checked experimentally.

Findings: The binary and ternary phase diagrams for studied surfactant mixtures include phase domains: mixed micelles; micelles + crystallites; crystallites, and molecular solution. The proposed general phase separation model for ionic surfactant mixtures is convenient for construction of such complex phase diagrams and provides information on the concentrations of all components of the complex solution and on the micellar electrostatic potential. The obtained maximal MES mole fraction of transparent micellar solutions could be of interest to increase the range of applicability of MES–surfactants.

* Corresponding author.
E-mail address: kd@lcpe.uni-sofia.bg (K.D. Danov).

https://doi.org/10.1016/j.jcis.2024.01.127
Received 14 November 2023; Received in revised form 7 January 2024; Accepted 18 January 2024
Available online 22 January 2024

1. Introduction

The global methyl ester sulfonate (MES or α-MES) market reached a volume of 0.91 million metric tons in 2022 and it is expected to grow to 1.5 million metric tons by 2026 [1–3]. The methyl ester sulfonates are oleo-chemical based anionic surfactants derived from renewable palm, coconut, or waste cooking oil through transesterification and subsequent sulfonation [4–9]. The interest of this surfactant class continuously grows because of the wide application in laundry, dishwashing, personal care, and pharmacy [2,4,5,8,10–22]. MES have excellent water hardness stability [13–15,18,19], biodegradability and biocompatibility [23] and are alternatives to the linear alkylbenzene sulfonates.

The physical properties of commercial palm-based MES surfactants are summarized in Ref. [24]. The rheological behavior of the mixed MES surfactant solutions [17], the oil drop deposition on solid surfaces [18], and their cleaning ability [19] have shown new possible wide practical applications. C*n*-MES molecules exhibit typical behavior for ionic surfactants [25–30]: the critical micelle concentration (CMC) decreases with the increase of number of carbon atoms in the alkyl chain, *n*, and with the salt concentration; the micelles are spherical with aggregation numbers from 57 (for C12-MES) to 90 (for C16-MES) for MES concentrations below 200 mM without added salt; C*n*-MES forms wormlike micelles with the rise of added salt concentration. The water hardness stability of MES solutions is explained with the comparable binding energy of Ca^{2+} and Na^{+} ions to the MES headgroup [4,28,31].

The methyl ester sulfonates are stable in the pH range from 4.5 to 9 [4,21] – for pH > 9, the hydrolysis phenomenon began to occur and the concentration of α-sulfo fatty acid di-Na salt gradually increases with storage time. For 16 and 18 carbon atoms in the MES alkyl chain, the respective Krafft temperature, T_K, increases from 28 °C for C16-MES to 41 °C for C18-MES [4,32]. In the literature [29,33], it is suggested to use the eutectic mixture of C16- and C18-MES (3/1 weight to weight fraction) in order to decrease the Krafft temperature to 15 °C. All C16-MES and C18-MES mixed solutions are turbid at large enough concentrations because of the formation of MES-crystals for temperatures lower than 15 °C. The ability of long chain length MES to form mixed micelles with nonionic surfactants, which do not precipitate at low temperatures, is shown that considerably increases the MES solubility [33]. The complex phase diagrams for MES + nonionic surfactant mixtures in terms of MES mole fraction, z_A, and total surfactant concentration, C_T, include phase domains: mixed micelles; micelles + crystallites; molecular solutions + crystallites; molecular solution.

The phase diagrams of fatty acids and alcohols in anionic and zwitterionic micellar surfactant solutions [35,36] were studied using the extended theoretical approach to model the micelle-monomer equilibria in complex surfactant solutions [34]. From this model, it follows that the number of phase domains and quadruple points rises when the surfactant solutions contain more than one partially soluble component, e.g. mixtures of C16-MES and C18-MES [33]. In the case of MES + anionic surfactant mixtures, the mixed micelles are charged and one expects lower MES solubility because of the higher free monomer MES concentration – the electrostatic repulsion between charged micelles and charged monomer MES molecules takes place. Second, the rise of the bulk concentration of counterions, e.g. Na^{+} ions, with C_T favors the formation of MES-crystals and should decrease the MES solubility.

Our goal in the present study is to generalize the phase separation model [34], applied in nonionic approximation for MES + nonionic surfactant mixtures [33], for MES + anionic surfactant mixtures accounting for the electrostatic interactions and counterion binding effect (Section 3). The theoretical model is checked by the measurements of the saturation mole fractions and electrolytic conductivity of MES in sodium lauryl ether sulfate with two ethylene oxide groups (SLES-2EO) and in sodium alpha olefin sulfonate (AOS) mixed surfactant solutions (Section 4). The completed set of experimental data allows calculating all of the needed physicochemical constants of MES and anionic surfactants in the bulk and micelles. The calculated 2D (one MES component) and 3D (two MES components) phase diagrams are summarized in Sections 5 and 6, respectively. Significant differences between nonionic approximation and the detailed theory are illustrated. It is shown that anionic surfactants SLES-2EO and AOS can be used to increase the solubility of MES at low temperature of 5 °C.

2. Materials and methods

All aqueous solutions were prepared with deionized water (Elix 3 purification system, Millipore, USA). The concentrated surfactant solutions were mixed and stirred at 40 °C for 1 h for the better solubility of all components, cooled down and placed in a thermostat at 25 °C or 5 °C at least for 24 h for equilibration.

Palmitic (C16-MES, M_w = 372 g/mol) and mixtures of palmitic and stearic (C18-MES, M_w = 400 g/mol) with C16-MES/C18-MES weight to weight fractions 80/20 and 60/40, produced by KLK OLEO, were used (Fig. 1). In all experiments, the pH of MES solutions is about 5.5 (adjusted if needed) in order to avoid the disalt formation. The active substances of C16-MES/C18-MES mixtures are > 92 %. The purity of C16-MES is 99.1 %, 100 mM C16-MES sample contains 24 ± 0.5 mM NaCl, and the CMC at 25 °C measured by the electrolytic conductivity is 1.02 ± 0.03 mM [26]. To check the values of the CMC and the amount of NaCl in mixed MES samples, the electrolytic conductivity vs the total surfactant concentration was measured by Hanna EC215 conductivity meter. The obtained results are: 100 mM C16-MES/C18-MES (80/20) sample contains 29 ± 0.7 mM NaCl; 100 mM C16-MES/C18-MES (60/40) sample contains 24 ± 0.6 mM NaCl; the CMCs are about 0.5 ± 0.02 mM (see Figs. S1 and S2).

The ability of two anionic surfactants to increase the MES solubility at low temperature of 5 °C was studied (Fig. 1). AOS (NANSA® LSS 495/H product of Innospec Performance Chemicals) is an anionic surfactant with number of carbon atoms 14–16, average molecular weight 320 g/mol, natural pH = 4.7, > 95 % active (Figs. 1 and S3). The kink point at 3.6 ± 0.06 mM in the electrolytic conductivity, κ_s, vs surfactant concentration of AOS (Fig. 2a) coincides with the CMC of pure AOS [37]. The calculated slope of the conductivity vs C_T is equal to 86.8 ± 0.8 S cm^2mol^{-1}, which corresponds to 12 ± 0.2 mM NaCl per 100 mM AOS

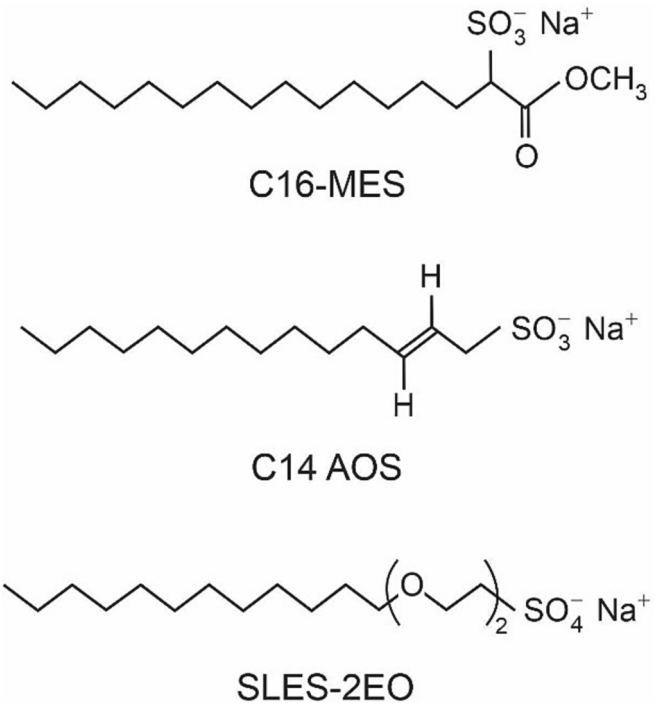

Fig. 1. Structural formulae of C16-MES, C14 AOS, and SLES-2EO.

(for details see Supplementary material). The experimental surface tension isotherm of aqueous AOS solutions is measured at 5 °C by force tensiometer K100 (Krüss, Germany) using the Du Noüy ring. The CMC obtained from the static measurements of the surface tension, σ, is 1.26 ± 0.05 mM (Fig. 2b), so that the AOS sample contains traces of nonionic surface-active admixture. The saturation adsorption at the CMC, Γ_{CMC}, is 2.83 ± 0.03 μmol/m^2, which is close to the experimental data reported in Ref. [37].

The second used anionic surfactant is SLES-2EO (ECOSOL® N 702 U product of PT Indo Sukses Sentra Usaha) with molecular weight 378 g/mol and active substance > 70 %. The natural pH of aqueous SLES-2EO solutions is 5 for surfactant concentrations above the CMC (Fig. S3). The measured electrolytic conductivity of the respective solutions is shown in Fig. 2a. One sees that the slope of the conductivity vs concentration below the CMC is equal to 70.4 ± 0.7 S cm^{2}mol^{-1}. Thus, the used sample is salt free from the viewpoint of the electrolytic conductivity measurements. The kink point in the conductivity data in Fig. 2a is at SLES-2EO concentration equals to 2.83 ± 0.04 mM. The obtained CMC coincides with the CMC of pure SLES-2EO aqueous solution [38]. The static surface tension measurements at 5 °C (see Fig. 2b) show that the CMC of SLES-2EO is lower (0.607 ± 0.007 mM) most probably because of the traces of unsulfated materials containing in the SLES-2EO sample. The saturation adsorption of 2.35 ± 0.04 μmol/m^2 is close to the experimental data reported in Ref. [38]. We estimated that even 1 % of nonionic surface-active admixtures are enough to decrease the CMC of pure compounds to the measured values for SLES-2EO and AOS. All studied concentrations are well above the CMC. Thus, the mixed micelles contain less than 1 % nonionic components and the obtained solubility data are correct.

The solubility of C*n*-MES depends on the bulk concentration of Na^+ ions coming from the dissociation of any added anionic surfactants and amount of NaCl in samples (Fig. S4a). To obtain the solubility concentrations at 5 °C, we measured the absorbance of light by a spectrometer (Jasco V-730) at wavelength $\lambda = 500$ nm. The flask with the probe was shaken before each absorbance measurement to disperse the available precipitates (if any). The increase of the turbidity with the rise of MES concentration is due to light scattering by MES crystallites at large enough concentrations. Because of the chemical equilibrium between MES in the monomeric form and free Na^+ ions and those incorporated in the precipitates, the sum of their electrochemical potentials is a constant which defines the solubility product of C*n*-MES [39,40]. The square roots of the solubility products are equal to the solubility-limit constants: 3.01 ± 0.03 mM for C14-MES; 0.749 ± 0.004 mM for C16-MES; 0.202 ± 0.002 mM for C18-MES (for details see Supplementary material, Fig. S4b, and Table S1).

All micellar anionic surfactant solutions are initially transparent at 5 °C and one day storage is enough to ensure the constant turbidity of individual MES solutions [33]. In contrast, the turbidity of mixed micellar solutions changes rather slowly over the storage time (Figs. S5). In these cases, all solutions were kept in a constant climate chamber (Binder KBF-S240) at 5 °C for the long-term storage (at least 3 months) to determine the boundary concentrations between the last clear and the first turbid solutions. To check if the obtained results correspond to the equilibrium reversible thermodynamic processes, all solutions (transparent and turbid at 5 °C) were heated up to 40 °C and cooled down to 25 °C – as a result all solutions become transparent. The subsequent storage of these solutions at 5 °C reproduced the turbidity data.

3. Theoretical model

In our previous study [33], the 2D and 3D phase diagrams were calculated for MES + nonionic surfactant mixtures. We approximately treated the mixed micelles as nonionic with effective micellization constants. This simpler approach will be further termed the *nonionic approximation*. Here, we generalize the phase separation model on the basis of the detailed theory of mixed micellar solutions of ionic surfactants [34] accounting for the possibility of one or more components to form precipitates [36,40]. Hereafter, it will be termed the *detailed theory*. The proposed model is based on a full system of equations that are expressing: (i) mass balances with respect to each component; (ii) chemical equilibria between micelles and monomers; (iii) chemical equilibria between monomers and precipitates (if any); (iv) the mechanical balance equation by Mitchell and Ninham [41], which states that the electrostatic repulsion between the headgroups of the ionic surfactant is counterbalanced by the attractive forces between the surfactant molecules in the micelles.

One considers a three-component ionic surfactant solution: C16-MES – component 1; C18-MES – component 2; ionic surfactant (SLES-2EO or AOS) – component 3. The counterion of all surfactants is Na^+ (component M) and the salt in the samples is NaCl. The input surfactant concentrations are C_j ($j = 1, 2, 3$) and the total input surfactant concentration is $C_T = C_1 + C_2 + C_3$. The phase diagrams are convenient to be presented in terms of C_T and mole fraction of MES molecules $z_A = (C_1 + C_2)/C_T$. The relative amount of salt in the samples with respect to the surfactant concentrations are r_j ($j = 1, 2, 3$): 0.24 for C16-MES and C16-MES/C18-MES (60/40); 0.29 for C16-MES/C18-MES (80/20); 0.12 for AOS; 0 for SLES-2EO (see Section 2). Thus, the input total salt concentration is $C_{salt} = r_1C_1 + r_2C_2 + r_3C_3$ and the input total counterion concentration is $C_M = C_T + C_{salt}$.

Generally, the solutions contain: free surfactant and counterion molecules in monomeric form with concentrations c_j ($j = 1, 2, 3$) and c_M,

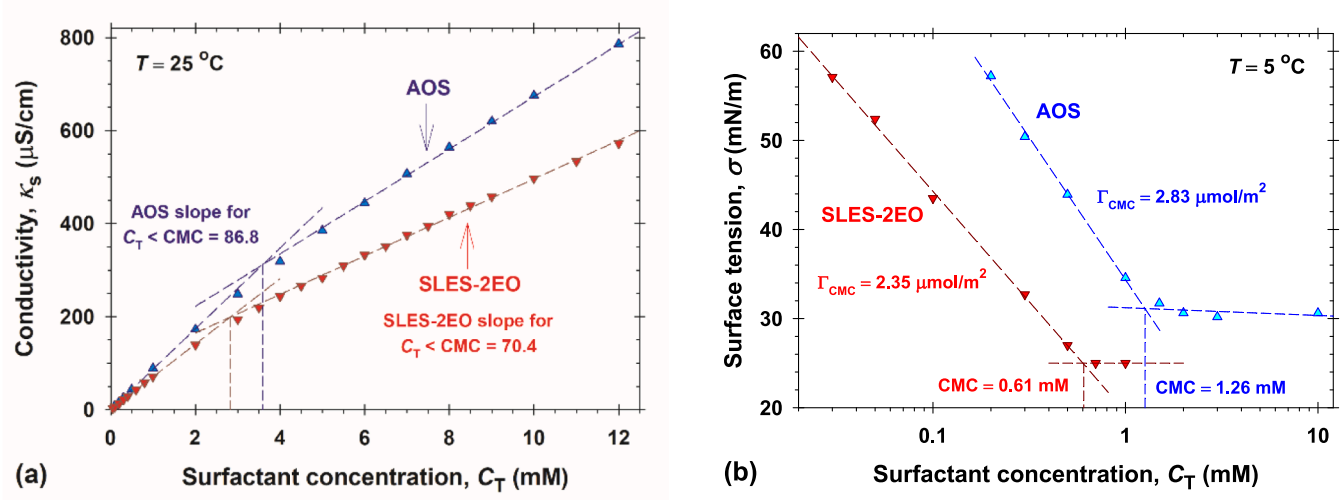

Fig. 2. Electrolytic conductivity (a) and surface tension (b) of AOS and SLES-2EO solutions vs surfactant concentration.

respectively; mixed micelles with total number of surfactant molecules c_{mic}; precipitates (if any) with total number of molecules incorporated in them $m_1 \geq 0$ for C16-MES, $m_2 \geq 0$ for C18-MES, and $m_3 = 0$ because AOS and SLES-2EO do not form precipitates at 5 °C. Only MES molecules can precipitate, they do not form mixed crystallites [33], and the total amount of MES molecules in the precipitates is $m = m_1 + m_2$. The mole fractions of the surfactant molecules incorporated in the mixed micelles are y_j ($j = 1, 2, 3$) and $y_1 + y_2 + y_3 = 1$. The counterion binding effect to the charged micelles is accounted for in the considered detailed model. The mole fractions of the surfactant molecules with bound counterions incorporated in the micelles are z_{Mj} ($j = 1, 2, 3$) and the total mole fraction of the bound counterions to mixed micelles is $z_M = z_{M1} + z_{M2} + z_{M3}$. Finally, the mole fractions of the surfactant molecules in the micelles without bound counterions are z_j ($j = 1, 2, 3$) and so that $z_j + z_{Mj} = y_j$ ($j = 1, 2, 3$). Thus, the mass balances for the surfactant and counterion molecules are described respectively by the following equations:

$$c_j + y_j c_{mic} + m_j = C_j \quad (j = 1, 2, 3) \tag{1}$$

$$c_M + z_M c_{mic} + m = C_M \tag{2}$$

The chemical potentials of the surfactant molecules in a monomeric form and those incorporated in the micelles are equal. Hence, the chemical equilibria lead to the following relationships:

$$\ln(\gamma_{\pm} c_j) = \ln K_j + \Phi_s + \ln(f_j z_j) \quad (j = 1, 2, 3) \tag{3}$$

here: e is the electronic charge; k_B is the Boltzmann constant; T is the absolute temperature; ψ_s is the surface electrostatic potential of micelles; $\Phi_s = |e\psi_s/(k_B T)| > 0$ is the dimensionless electrostatic potential; $\gamma_{\pm}$ is the activity coefficient in the bulk phase; f_j and K_j are the activity coefficient and the micellar constant of the j-th surfactant in the micellar phase, respectively.

The localized (Langmuirian type) adsorption of Na^+ counterions on the j-th ionic-surfactant headgroup is described by the Stern adsorption isotherm with Stern constant $K_{St,j}$ ($j = 1, 2, 3$), respectively [34,42,43]. Hence, this counterion binding mechanism leads to the following result:

$$\ln(K_{St,j} \gamma_{\pm}^2 c_M c_j) = \ln K_j + \ln(f_j z_{Mj}) \quad (j = 1, 2, 3) \tag{4}$$

The adsorption binding energy of Na^+ counterion to sulfate headgroup is lower than that to sulfonate headgroup and the respective values of the Stern constants are: $K_{St,1} = K_{St,2} = 2.86 \times 10^{-3}$ $(mM)^{-1}$ [26]; $K_{St,3} = 2.86 \times 10^{-3}$ $(mM)^{-1}$ for AOS [26]; $K_{St,3} = 6.53 \times 10^{-4}$ $(mM)^{-1}$ for SLES-2EO [42,43].

The activity coefficient in the bulk phase is calculated from the bulk ionic strength, $I = (c_1 + c_2 + c_3 + c_M + C_{salt})/2$, in which the micelles do not contribute. The following semi-empirical expression:

$$\log_{10}\gamma_{\pm} = 0.055I - \frac{0.5115 I^{1/2}}{1 + 1.316 I^{1/2}} \tag{5}$$

which originates from the Debye-Hückel theory, is widely used in the literature [26,43,44] for 1:1 electrolytes. The ionic strength in Eq. (5) is measured in M.

The classical regular solution theory [45] relates the activity coefficients in the micellar phase with the interaction energies between molecules and mole fractions in the micelles for two component systems. We extended the Rubingh approach for a three-component system (see Section S2) and derived the following expressions for the activity coefficients, f_j, in the micellar phase:

$$\ln f_j = \beta_{ji} y_i^2 + \beta_{jk} y_k^2 + (\beta_{ji} + \beta_{jk} - \beta_{ik}) y_i y_k \quad (j = 1, 2, 3) \tag{6}$$

Here: $\beta_{ik} = \beta_{ki}$ is the dimensionless interaction parameters between the i-th and k-th molecules in the micellar phase; (i, j, k) is a given permutation of (1, 2, 3). For example, if $j = 3$, then $i = 1$ and $k = 2$ or $i = 2$ and $k = 1$ – in both cases, Eq. (6) has an equivalent form because of the symmetry, $\beta_{ik} = \beta_{ki}$. The negative values of β_{ik} correspond to synergistic missing, the positive values of β_{ik} – to antagonistic mixing, and $\beta_{ik} = 0$ – to ideal mixing between the i-th and k-th components in the micellar phase. In the case of two components $y_3 = 0$ and the obtained result is reduced to the Rubingh formulae [45]: $f_1 = \exp(\beta_{12} y_2^2)$ and $f_2 = \exp(\beta_{12} y_1^2)$.

The system of equations describing the mass balances and chemical equilibria of components is not closed. If the non-electrostatic micelle tensions of the individual surfactants are γ_i ($i = 1, 2, 3$) and the electrostatic component of the 2D micelle tension is π_{el}, then the generalized expression for the Mitchell-Ninham closure for mixed micelles reads [34]:

$$\pi_{el} = f_1 y_1 \gamma_1 + f_2 y_2 \gamma_2 + f_3 y_3 \gamma_3 \tag{7}$$

The values of γ_i ($i = 1, 2, 3$) are given in the literature: $\gamma_1 = \gamma_2 = 3.65$ mN/m [26]; $\gamma_3 = 3.60$ mN/m [34] for AOS; $\gamma_3 = 4.30$ mN/m [34] for SLES-2EO. The measured viscosities of all solutions are low so that the shape of mixed micelles is close to spherical with radius R. In this case, the following expressions:

$$\pi_{el} = 16 k_B T \frac{I}{\kappa} \left\{ H \sinh^2\left(\frac{\Phi_s}{4}\right) - \nu \frac{\Phi_s}{16} \frac{\Phi_s - 4\tanh(\Phi_s/4)}{H \sinh(\Phi_s/2)} + \frac{2}{\kappa R} \ln\left[\cosh\left(\frac{\Phi_s}{4}\right)\right] \right\} \tag{8}$$

$$H = \left[1 + \nu \frac{\sinh(\Phi_s) - \Phi_s}{\cosh(\Phi_s) - 1}\right]^{1/2}$$
$$\nu = \frac{c_M - c_1 - c_2 - c_3 - C_{salt}}{c_M + c_1 + c_2 + c_3 + C_{salt}} \tag{9}$$

for the electrostatic component of the micelle tension are derived in the literature [34]. If the dielectric permittivity in vacuum is ε_0, the relative dielectric permittivity is ε, and the bulk ionic strength is I, then the Debye parameter, κ, in Eq. (8) is calculated as follows:

$$\kappa^2 = \frac{2 e^2 I}{\varepsilon_0 \varepsilon k_B T} \tag{10}$$

In the case without precipitates, $m_j = 0$ ($j = 1, 2, 3$), the considered system of equations is closed and all concentrations, mole fractions and the electrostatic potential can be calculated. Note that C16-MES and C18-MES can form precipitates when the respective solubility-limit constants, S_j ($j = 1, 2$), are reached (see Section S1). The estimated experimental values of S_1 and S_2 are: $S_1 = 0.749$ mM for C16-MES; $S_2 = 0.202$ mM for C18-MES. In the case of one or two precipitates, $m_1 > 0$ and/or $m_2 > 0$, the conditions for the respective solubility limits close the system of equations:

$$\gamma_{\pm}^2 c_M c_1 = S_1^2 \quad \text{and/or} \quad \gamma_{\pm}^2 c_M c_2 = S_2^2 \tag{11}$$

Generally, the phase diagrams of these solutions can contain following domains: molecular solutions; molecular solutions with one or two MES precipitates; micellar solutions without precipitates; micellar solutions with one or two MES precipitates. All needed physicochemical parameters in the detailed model are known except for the micellar constants, K_j ($j = 1, 2, 3$), and the interaction parameters, β_{12}, β_{13}, and β_{23}. The values of these parameters are obtained from the experimental data for the solubility of MES in the ionic cosurfactant solutions with different concentrations C_3 (Section 4).

4. Determination of the micellar constants and the dimensionless interaction parameters

In the case of individual AOS or SLES-2EO solutions, the micellar constants are obtained in Section S3 based on the electrolytic conductivity measurements (Fig. 2a) and the simplified version of the detailed model (Section 3) for ionic surfactant solutions without added MES: $K_3 = 0.0576 \pm 0.0004$ mM for AOS; $K_3 = 0.169 \pm 0.004$ mM for SLES-2EO.

The micellar constants for hexadecanol and octadecanol in the mixed micelles with SLES and cocamidopropyl betaine (CAPB) at different temperatures are obtained experimentally in Ref. [36]. From the dependence of these micellar constants on temperature, we calculated their values at $T = 5$ °C (see Section S3 and Fig. S6). We assume that the difference between the standard chemical potentials of molecules in a monomeric form (in the bulk phase) and those in the micellar phase for hexadecanol (octadecanol) is close to that for C16-MES (C18-MES) because their polar heads stay in the water and the hydrocarbon tails are identical. As a result, the following most probable values of the micellar constants are calculated in Section S3: $K_1 = 5.7 \pm 0.2$ μM for C16-MES; $K_2 = 0.44 \pm 0.02$ μM for C18-MES. The calculated values for the micellar constants show that $\ln(K_3/K_1) = 3.39$ for SLES-2EO and $\ln(K_3/K_1) = 2.31$ for AOS – the relative increase of the micellization energy in k_BT units for SLES-2EO is greater than that for AOS because the number of the carbon atoms in the hydrocarbon tail of SLES-2EO is 12 and that for AOS is 14–16 [46].

The mixing of C16-MES and C18-MES molecules in micelles is ideal [33] and the interaction parameter β_{12} is equal to zero. Thus, the only unknown parameters in the detailed model are the interaction parameters between MES and the ionic cosurfactant molecules, β_{13} and β_{23}.

To obtain the experimental value of the interaction parameter, β_{13}, we measured the C16-MES concentrations of the last clear and the first turbid mixed surfactant micellar solutions for different concentrations of AOS and SLES-2EO (Fig. S5) after a long-term storage in a constant climate chamber (Section 2). The experimental data (symbols) are summarized in Fig. 3a and 3b. According to the nonionic approximation [33], C_1 vs C_T should be a straight line with a slope and an intercept depending on the saturation mole fraction of C16-MES in mixed micelles (Section S3). The obtained most probable values of the saturation mole fractions (0.18 ± 0.01 for both SLES-2EO and AOS mixed micelles) seem to be reasonable but the description of the experimental data is not so good. Thus, the nonionic approximation can be used for a qualitative comparison between solubility results for ionic cosurfactants but it fails down for a precise construction of the solution phase diagrams.

The solid lines in Fig. 3a and 3b are drawn using the detailed theory (Section 3) simplified for the C16-MES + ionic surfactant solutions and for the phase boundary between micellar solutions without and micellar solutions with C16-MES precipitates: i) $C_2 = 0$; ii) $m_1 = m_2 = 0$; iii) $c_{mic} > 0$. All physicochemical parameters are defined and the solid lines in Fig. 3a and 3b are drawn using *one adjustable parameter*, β_{13}. The detailed theory describes excellently the experimental data and the obtained most probable values of β_{13} are: $\beta_{13} = 0.49 \pm 0.01$ for C16-MES in SLES-2EO; $\beta_{13} = 0.44 \pm 0.01$ for C16-MES in AOS.

The detailed model predicts the electrostatic surface potential of micelles and all concentrations. Fig. 3c, 3d, and S7 summarize the calculated results for the degree of counterion binding, for ψ_s, and for the surfactant monomer concentrations in the bulk, c_1 and c_3, respectively. Typically for ionic micellar solutions [34], the degree of counterion binding increases and the magnitude of the electrostatic potential decreases with the rise of ionic strength. Because of the lower counterion binding energy in the case of sulfate polar head, the degree of counterion binding in the case of SLES-2EO is lower than that for mixed AOS micelles, see Fig. S7a and 3c. The bulk monomer concentration of C16-MES ions, c_1, and that of cosurfactant ions, c_3, decrease with the total surfactant concentration (Fig. 3d and S7b) – the incorporation of these ions in the mixed micelles is favored with the decrease of the electrostatic repulsion.

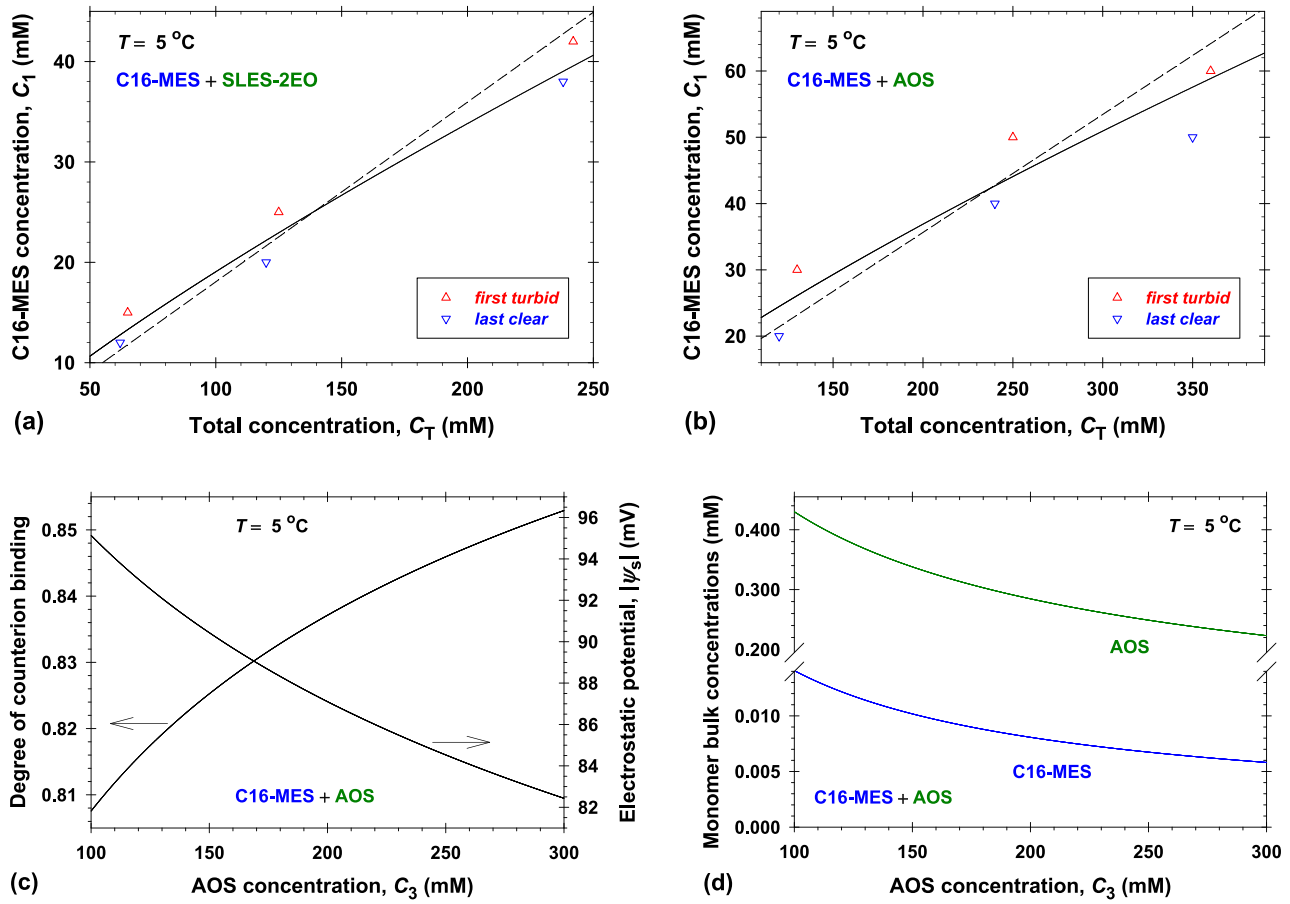

Fig. 3. Dependence of the C16-MES concentrations, C_1, of the last clear and the first turbid solutions on the total surfactant concentration, C_T: (a) C16-MES + SLES-2EO; (b) C16-MES + AOS. The dashed lines correspond to the nonionic approximation and the solid lines describe the result from the detailed theory. Calculated degree of counterion binding and electrostatic potential (c) and monomer bulk concentrations (d) along the phase boundary for C16-MES + AOS micellar solutions.

To obtain the C18-MES micellar constants, one uses the following strategy for data processing of the solubility in the case of C16-MES/C18-MES (60/40) + ionic surfactant mixed micellar solutions. We assume that C18-MES precipitates first and apply the nonionic approximation approach to obtain the most probable values of the saturation mole fraction of C18-MES in mixed micelles (Section S3). The dashed lines in Fig. 4a and 4b are plotted with the values 0.093 ± 0.001 and 0.062 ± 0.001 for SLES-2EO and AOS, respectively. Again, the description of experimental data is not good. Further, we applied the detailed model in which: i) the concentration, $s_2 = (\gamma_{\pm}^2 c_M c_2)^{1/2}$, of C18-MES is equal to the solubility-limit constant, S_2, at the phase boundary micellar solution/micellar solution + one precipitate [26]; ii) $m_1 = m_2 = 0$; iii) $c_{mic} > 0$. All parameters of the detailed model are known except for the interaction parameter between C18-MES and ionic cosurfactant molecules in the micellar phase, β_{23}. The experimental data in Fig. 4a and 4b are fitted using *one adjustable parameter*, β_{23}. As a result, $\beta_{23} = 1.63 \pm 0.01$ for AOS, $\beta_{23} = 1.35 \pm 0.01$ for SLES-2EO, and the respective best theoretical calculations (solid lines) explain excellently the experimental data. As should be, the concentration, $s_1 = (\gamma_{\pm}^2 c_M c_1)^{1/2}$, of C16-MES is lower than the solubility-limit constant, S_1. Fig. 4c, 4d, and S8 summarize the obtained dependencies of the micellar and bulk parameters on the ionic surfactant concentration, C_3. The general trends are similar to those illustrated in Fig. 3c, 3d, and S7. The degree of counterion binding and the magnitude of the electrostatic potential are slightly higher for C16-MES/C18-MES (60/40) mixed micelles compared to C16-MES mixed micelles. Fig. 4d and S7b show that the bulk monomer concentration of C18-MES, c_2, is considerably lower than that of C16-MES, c_1. Nevertheless, the C18-MES precipitates first because of $S_2 < S_1$.

To prove the validity of the detailed theory predictions, one uses the experimental data for C16-MES/C18-MES (80/20) + ionic surfactants (Fig. 5). All needed physicochemical parameters are already determined and the solid lines in Fig. 5 are drawn without adjustable parameter. The excellent description of the boundaries between the first turbid and last clear solutions is illustrated assuming that C16-MES precipitates first. The dot-dashed lines show the dependence of concentration s_2 for C18-MES on C_T. As should be for all studied concentration $s_2 < S_2$. The calculated dependencies of the micellar and bulk parameters on the ionic surfactant concentration, C_3, are given in Figs. S9 and S10.

It is interesting to note, that the nonionic approximation curves (dashed lines) with the obtained values of the saturation mole fractions of MES qualitatively follow the experimental data (Section 3). Nevertheless, the addition of NaCl leads to the change of turbidity of surfactant solutions and as a result, one should obtain the new experimental values of the saturation mole fractions of MES in order to apply the simpler nonionic approximation. In contrast, the detailed model accounts for the effect of Na^+ counterions and it can predict the corresponding phase diagrams without the need of additional experiments.

5. C16-MES and C18-MES phase diagrams

In the case of one MES component and ionic cosurfactant mixture, the phase diagram contains *four domains*: molecular solution; molecular solution + MES crystals; micellar solution + MES crystals; micellar solution without precipitates. These domains are separated by four phase boundaries, which intersect into quadrupole point Q (Figs. 6 and 7). The detailed model (Section 3) predicts the solution properties for all values of the MES mole fraction, z_A, and the input total surfactant

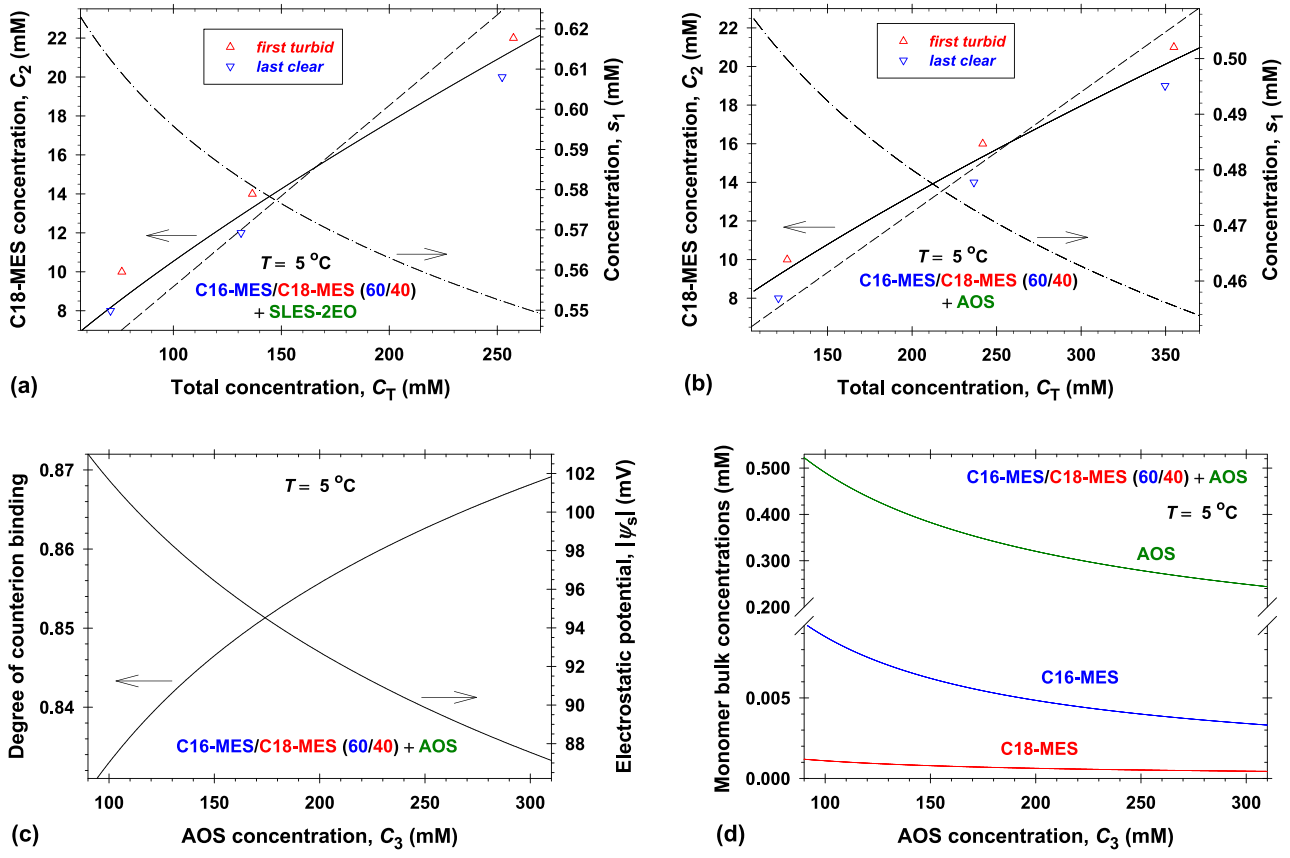

Fig. 4. Dependence of the C18-MES concentrations, C_2, of the last clear and the first turbid solutions and concentration s_1 on the total surfactant concentration, C_T: (a) C16-MES/C18-MES (60/40) + SLES-2EO; (b) C16-MES/C18-MES (60/40) + AOS. The dashed lines correspond to the nonionic approximation and the solid lines describe the result from the detailed theory. Calculated degree of counterion binding and electrostatic potential (c) and monomer bulk concentrations (d) along the phase boundary for C16-MES/C18-MES (60/40) + AOS micellar solutions.

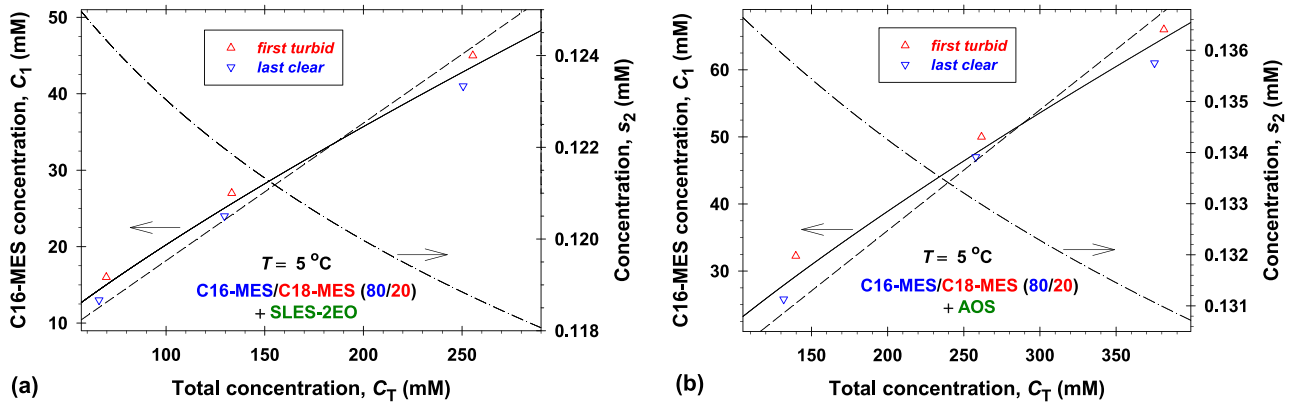

Fig. 5. Dependence of the C16-MES concentrations, C_1, of the last clear and the first turbid solutions and concentration s_2 on the total surfactant concentration, C_T: (a) C16-MES/C18-MES (80/20) + SLES-2EO; (b) C16-MES/C18-MES (80/20) + AOS. The dashed lines correspond to the nonionic approximation and the solid lines describe the result from the detailed theory.

concentration, C_T. The respective phase boundaries are calculated as follows ($k = 1$ stands for C16-MES and $k = 2$ for C18-MES). For example, in the case of C16-MES + ionic surfactant, the concentration of C18-MES, C_2, is equal to zero, and oppositely for C18-MES solutions, $C_1 = 0$.

Molecular solution/micellar solution (D-line). This phase line describes the critical micelle concentration of the mixed solutions. In the general model, one substitutes: $m_k = 0$ (no precipitates); $c_{mic} = 0$ (the number of micelles at the D-line is equal to zero). As a result, we obtained $z_A = z_A(C_T)$ and concentration $s_k = s_k(C_T)$. The calculations are performed for $s_k < S_k$ and they are stopped at quadrupole point Q, where s_k is equal to the solubility-limit constant, S_k.

Molecular solution/molecular solution + MES crystals (C-line). There are no micelles at this boundary ($c_{mic} = 0$) and the bulk monomer concentrations are equal to the input MES, ionic surfactant, and dissociated Na^+ ions concentrations. Thus, the C-line is described by the solubility-limit constant of MES, $s_k = S_k$.

Micellar solution/micellar solution + MES crystals (A-line). The calculations along this phase boundary are described in Section 4. In fact, they start from the total surfactant concentration corresponding to the quadrupole point, Q, and C_T increases to obtain the respective dependence $z_A = z_A(C_T)$.

Molecular solution + MES crystals/micellar solution + MES crystals (B-line). The detailed model is applied for: $c_{mic} = 0$ (the number of micelles at the B-line is equal to zero); $m_k > 0$ (there are MES precipitates); $s_k = S_k$ (the bulk monomer MES concentration is controlled by the bulk solubility of MES).

Fig. 6 shows the phase diagrams of C16-MES in (a) SLES-2EO and (b) AOS mixed solutions. The experimental points corresponding to the last clear (▽) and the first turbid (△) solutions (Fig. 3a and 3b) are plotted in terms of $z_A = z_A(C_T)$ and as should be, the respective A-lines passes through them. To verify the positions of the B- and C-lines, we measured the dependencies of the electrolytic conductivity of solutions for fixed MES mole fractions, $z_A = 0.7$ and $z_A = 0.8$, on the total surfactant concentration, C_T, at 5 °C (Figs. S11 and S12). With the rise of C_T, the slope of the conductivity vs C_T in the molecular solution + C16-crystals domain decreases compared to that in the molecular solution domain because of the C16-MES precipitates. The subsequent increase of C_T, leads to the second kink point in the conductivity measurements – as a result of the formation of micelles and counterion binding to them, the conductivity data slope in the micellar solution + C16-crystals decreases. The respective positions of the kink points of the conductivity data (□) are excellently described by the phase boundaries (B- and C-lines) in Fig. 6.

With the rise of the nonionic cosurfactant concentration along the A-line, the MES mole fraction, z_A, slightly decreases to a given constant value corresponding to the solubility limit mole fraction of MES in the mixed micelles [33]. In the case of ionic cosurfactants, the most intriguing result is the maximum of z_A vs C_T ($z_A = 0.248$ for $C_T = 11.1$ mM for SLES-2EO and 0.272 at 14.1 mM for AOS) along the A-line (Fig. 6), which needs a further explanation. First, the number of molecules of MES incorporated in the mixed micelles increases with the ionic surfactant concentration, C_3. Nevertheless, the mole fraction of MES, z_A,

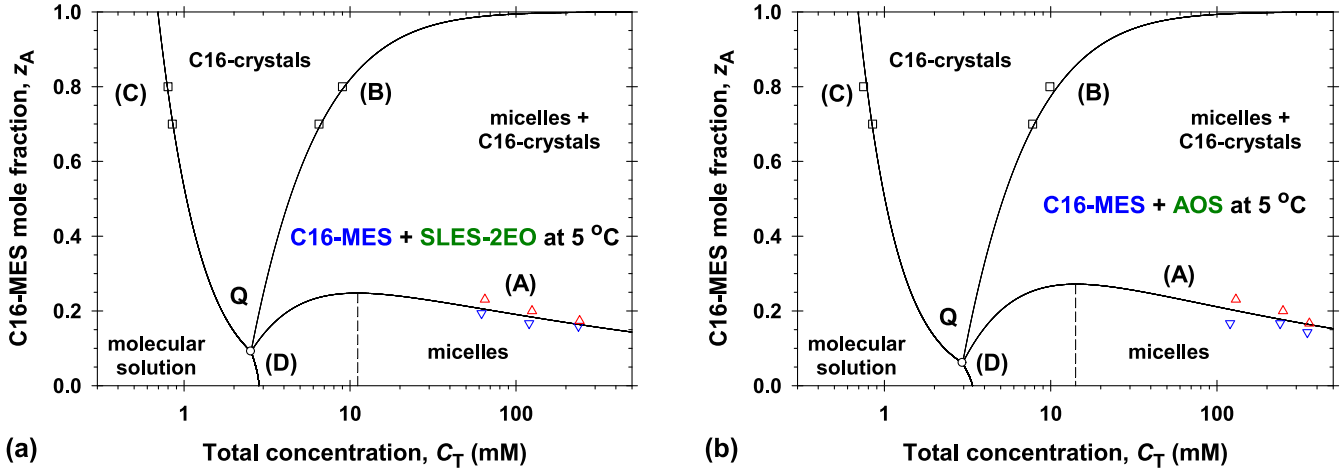

Fig. 6. Phase diagrams of C16-MES in (a) SLES-2EO and (b) AOS mixed solutions. The experimental points correspond to the last clear and the first turbid solutions (Fig. 3a and 3b) and to the positions of the kinks in the electrolytic conductivity vs C_T data (Figs. S11 and S12), which were measured to verify the phase diagrams.

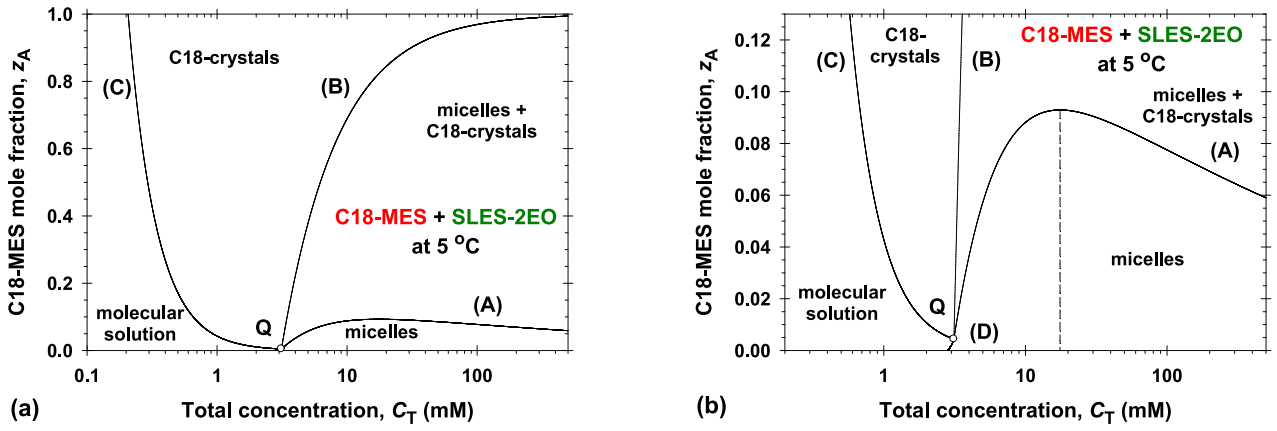

Fig. 7. (a) Phase diagram of C18-MES + SLES-2EO micellar solutions. (b) Enlarged view of the phase diagram around the quadrupole point, Q.

is bounded by the saturation mole fraction of MES in mixed micelles. Second, the increase of C_3 gives rise of the concentration of the not bound Na^+ counterions to the micelles, c_M (Fig. S13): i) the increase of c_M favors the precipitation of MES; ii) the larger ionic strength suppresses the electrostatic repulsion between the dissociated MES molecules in the bulk and the micelles, decreases the magnitude of the micellar electrostatic potential, and the free monomer MES concentration. The maximums of z_A along the A-line are results of the counterbalance between the last two trends.

The energies of counterion binding are important for the values and the positions of the maximums in Fig. 6. The SLES-2EO sample is salt free and that of AOS contains 12 mM NaCl per 100 mM AOS (Section 2). Nevertheless, because of the higher energy of Na^+ counterion binding to the sulfonate group compared to that to the sulfate group, the degree of counterion binding is higher and the respective concentration of free Na^+ ions is lower for C16-MES + AOS compared to C16-MES + SLES-2EO mixed solutions (see Fig. S13). This explains the greater value of the z_A-maximum at higher C_T in the case of AOS compared to that in the case of SLES-2EO.

The detailed model also predicts the 2D phase diagrams of C18-MES in SLES-2O (Fig. 7) and in AOS (Fig. S14) mixed micellar solutions. In our calculations, we assumed that the C18-MES sample is salt free. The solubility of C18-MES is considerably lower than that of C16-MES and the concentration of counterions around the CMC is high – as a result the position of the quadrupole point is close to the CMC of ionic cosurfactant without added MES (Fig. 7b). The physical explanation of the maximum of the MES mole fraction along the A-line is analogous to that in the case of C16-MES: $z_A = 0.0929$ at $C_T = 17.6$ mM for C18MES + SLES-2EO (Fig. 7b); $z_A = 0.0718$ at $C_T = 20.9$ mM for C18MES + AOS (Fig. S14b). Note that the maximum value of z_A for C18MES + SLES-2EO is greater than that for C18MES + AOS, while the difference between the values of these maximums for C16-MES is small (Fig. 6). The dependencies of the micellar parameters along the A-lines on the cosurfactant concentration, C_3, are summarized in Fig. S15.

6. Phase diagrams of mixed C16-MES/C18-MES and ionic cosurfactant solutions

The phase diagrams for micellar solutions of two partially soluble components (e.g. C16-MES and C18-MES) in the presence of soluble cosurfactant (e.g. SLES or AOS) are three dimensional. For quantitative representation, it is convenient to plot 2D cross sections for fixed molar ratios between two of the components [33]. If the partially soluble components cannot form mixed precipitates, then the phase diagram can contain *eight different kinds of domains*: molecular solution; molecular solutions with one kind of precipitates (denoted as C16-crystals and C18-crystals) and with precipitates from the both of them (denoted as C16-C18-crysrals); micellar solution without precipitates (micelles); one kind of precipitates coexists with the micelles (denoted as micelles + C16-crystals and micelles + C18-crystals) and micellar solutions with precipitates of the two partially soluble components (denoted as micelles + C16-C18-crystals). The number of phase boundaries depends on the complexity of the respective 3D phase diagram.

Fig. 8 shows the calculated phase diagrams for C16-MES/C18-MES (60/40) micellar solutions in the presence of AOS (Fig. 8a) or SLES-2EO (Fig. 8b). The experimental points for the last clear (▽) and the first turbid (Δ) solutions (Fig. 4a and 4b) are included in Fig. 8 in order to demonstrate that they lay on the phase boundary micelles/micelles + C18-crystals. The enlarged views of these phase diagrams for low values of the MES mole fractions are presented in Section S5.

In the case of AOS. The type of the phase diagram illustrated in Fig. 8a is analogous to those for C16-MES/C18-MES (60/40) and nonionic cosurfactant solutions [33]. One starts the calculations from the CMC of the ionic cosurfactant (AOS), increases z_A, and calculates the position of the D-line (see Section 5). The calculations stop at quadrupole point Q1, where the solubility concentration s_2 is equal to the solubility-limit constant, S_2. The position of the quadrupole point Q1 is close to the CMC of AOS because of the low solubility of C18-MES (Fig. S16a). Subsequently, the calculations along the phase boundary molecular solution/C18-crystals (C1-line), micelles/micelles + C18-crystalls (A1-line), and micelles + C18-crystalls/C18-crystals (B1-line) are analogous to those described in Section 5. Note that along the B1-line, one increases the mole fraction of MES and calculates all physicochemical parameters including the solubility concentration of C16-MES, s_1. At the point, where solubility concentration s_1 is equal to the solubility-limit constant, S_1, both MES components precipitate and micelles appear. This defines the second quadrupole point, Q2. In fact, lines A2, B2, and *C*2 have analogous meaning to lines A1, B1, and C1 but with respect to the second MES component, which can precipitate (in our case C16-MES).

The maximal MES mole fraction of the transparent micellar solutions is equal to 0.311 at 12.6 mM total surfactant concentration. It is interesting to note, that this value of z_A (0.311) is greater than the maximum value of 0.272 for C16-MES + AOS (Fig. 6b).

In the case of SLES-2EO. The micellar parameters of SLES-2EO are not considerably different than that of AOS. The main difference is that SLES-2EO sample is salt free. One sees that the positions of quadrupole points Q1 and Q2 and lines B1, C1, *C*2, and D are not so different for SLES-2EO (Fig. 8b) compared to those for AOS (Fig. 8a) for low total surfactant concentrations, C_T. The main difference is that the A1-line starting from point Q1 and the A2-line starting from point Q2 intersect in the third quadrupole point, Q3. The respective A1-line and A2-line with the decrease of the total surfactant concentrations starting from high values of C_T (e.g. C_T = 500 mM) intersect in the fourth

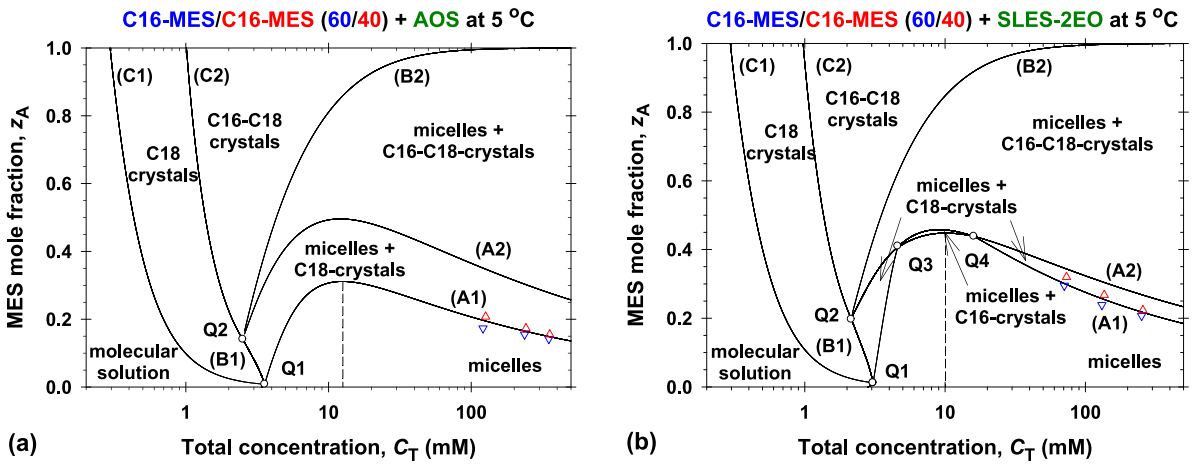

Fig. 8. Phase diagrams of C16-MES/C18-MES (60/40) in the presence of AOS (a) and in the presence of SLES-2EO (b). Symbols show experimental data from Fig. 4a and 4b and the dashed lines correspond to the transparent micellar solutions with maximal MES mole fractions.

quadrupole point, Q4. As a result, a small domain with micelles + C16-crystals is formed (Fig. 8b). For fixed C_T between 4.6 mM and 16 mM with the rise of z_A, one passes through domains micelles, micelles + C16-crystals, micelles + C16-C18-crystals and finally C16-C18-crystlas. Because of the lower ionic strength, the maximum of the MES mole fraction vs C_T is the highest, $z_A = 0.448$ at $C_T = 10.1$ mM.

Fig. 9 summarizes the obtained numerical results (solid lines) for the phase diagrams of C16-MES/C18-MES (80/20) solutions in the presence of AOS or SLES-2EO – the enlarged views for small MES mole fractions are presented in Fig. S17. For both ionic cosurfactants, the phase diagrams are quite similar but considerably different than those for lower fraction of C16-MES given in Fig. 8. Starting from the CMC of the individual ionic cosurfactant and increasing the MES mole fraction, z_A, one calculates the D-line. At this line, concentration s_2 increases and becomes equal to the solubility-limit constant, S_2, of C18-MES at quadrupole point Q1. This point belongs to the boundaries between domains molecular solution, C18-crystals, micelles + C18-crystals, and micelles. The subsequent increase of z_A describes a phase boundary between the molecular solutions with C18-MES precipitates and micellar solutions with C18-MES precipitates, which is analogous to the B1-line in Fig. 8a. This line starts from quadrupole point Q1 and ends at quadrupole point Q2. At the A1-line started from Q1, the solubility concentration of C16-MES, s_1, increases and it becomes equal to the solubility-limit concentration, S_1, at the third quadrupole point, Q3. Instead of the low weight fraction of C18-MES (20 %) in this MES sample, a region with mixed micelles and C18-crystals appears. In fact, the first C16-MES precipitate appears at quadrupole point Q3 corresponding to the boundaries between domains micelles, micelles + C16-crystals, micelles + C16-C18-crystals, and micelles + C18-crystals.

Starting from the large enough total surfactant concentration (e.g. $C_T = 500$ mM), the experimental A1-line describes the phase boundary between micellar solutions without and with C16-MES precipitates. As should be, the experimental data lay on the A1-line (Fig. 5). With the decrease of C_T along the A1-line, concentration s_2 increases and at quadrupole point Q3 becomes equal to the solubility limit-constant, S_2. The line between quadrupole points Q2 and Q3 is the phase boundary between micellar solutions with C18-MES precipitates and micellar solutions with precipitates of the both partially soluble components (Fig. S17).

The dashed lines in Fig. 9 correspond to the transparent micellar solutions with maximal possible MES mole fractions: $z_A = 0.354$ at $C_T = 14.2$ mM for AOS; $z_A = 0.298$ at $C_T = 11.3$ mM for SLES-2EO. It is interesting to note, that the greatest maximum value of z_A is obtained for C16-MES/C18-MES (80/20) in the presence of AOS, while that in the presence of SLES-2EO for larger amount of C18-MES in the mixture (60/40).

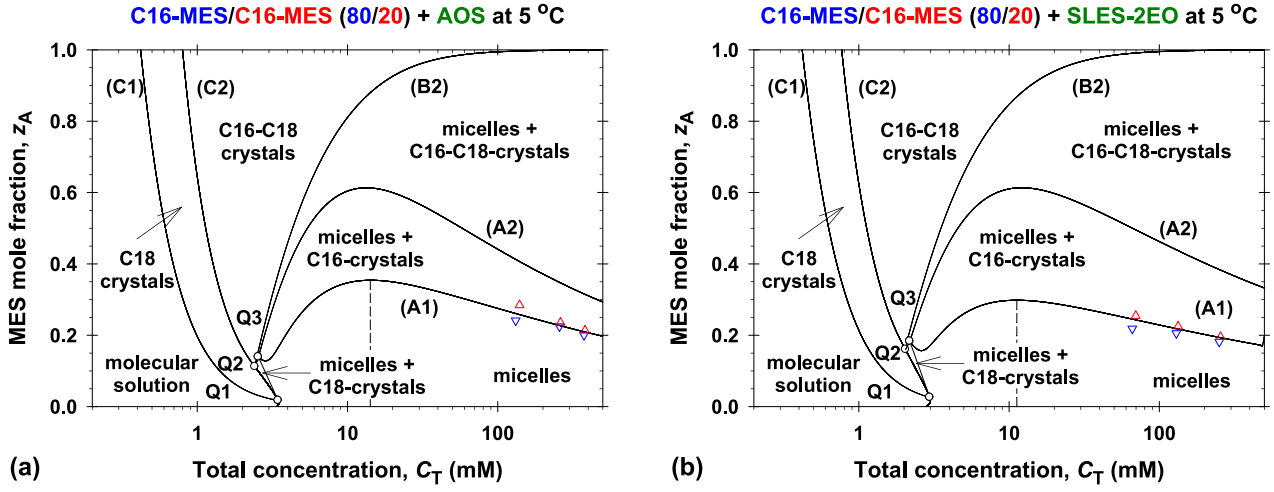

Fig. 9. Phase diagrams of C16-MES/C18-MES (80/20) in the presence of AOS (a) and in the presence of SLES-2EO (b). Symbols show experimental data from Fig. 5a and 5b and the dashed lines correspond to the transparent micellar solutions with maximal MES mole fractions.

7. Conclusions

The water solubility of long chain length methyl ester sulfonates (C16-MES and C18-MES) decreases significantly for temperatures below their Krafft points [4,29,32,33]. An efficient way to increase the MES solubility is to incorporate C16-MES and C18-MES in mixed micelles. The wide application of conventional anionic surfactants [47] opens the question on the solubility of MES in the presence of anionic cosurfactants.

The precise measurements of the turbidity of C*n*-MES and their mixtures in water at 5 °C showed that their solubility depends on the counterion concentration in the presence of NaCl. The logarithm of the solubility-limit constants, S_n, is a linear function of the number of carbon atoms, n, in the alkyl chain (Fig. S4b, and Table S1). The electrostatic repulsion between the charged ionic micelles and charged free MES molecules lowers the possibility of the incorporation of MES in the mixed micelles. With the rise of ionic cosurfactant concentration, the ionic strength increases: i) the micellar electrostatic potential decreases, which favors the incorporation of MES in the mixed micelles; ii) the counterion concentration increases, which lowers the MES solubility. The fine balance between these opposite trends is accounted for in the developed general phase separation model (Section 3).

To determine the needed model physicochemical parameters of the used MES, sodium alpha olefin sulfonate (AOS), and sodium lauryl ether sulfate with two ethylene oxide groups (SLES-2EO) samples, we measured the electrolytic conductivity and surface tension isotherms (Section 2). The micellar constants, energy of counterion binding to the micelles (Stern constants), the amount of NaCl in each sample are obtained. The experimental data for the solubility limit of C16-MES and mixed C16-MES and C18-MES solutions in the presence of AOS and SLES-2EO are fitted using one adjustable parameter – the interaction parameter, β_{13} and β_{23}, between MES and ionic cosurfactant molecules in the mixed micelles appearing in the regular solution approach (Section 4). The obtained positive values of $0 < \beta_{13} < \beta_{23}$ correspond to an antagonistic mixing of the components in the mixed micelles, which is more pronounced for C18-MES if compared to C16-MES.

The quantitative 2D phase diagrams for one partially soluble component (C16-MES and C18-MES) are calculated using the generalized phase separation model and verified experimentally (Figs. 6 and 7, Supplementary Material). They contain a typical four phase domains (molecular solution, micellar solution, molecular solution with MES precipitates, coexistence of micelles and MES precipitates), which are separated by four boundaries intersecting in one quadrupole point Q [33,35,36]. An important observation is the obtained maximal mole fraction of MES at a given total surfactant concentration of transparent micellar solutions. The relative maximum capacities of micelles are 0.248 and 0.272 for C16-MES in SLES-2EO and in AOS, respectively. As should be, these capacities for C18-MES are considerably lower: 0.0929 and 0.0718 in SLES-2EO and AOS, respectively.

In the case of mixtures C16-MES/C18-MES (60/40 and 80/20) and ionic cosurfactant, the respective cross sections of the 3D phase diagrams are calculated and verified experimentally (see Figs. 8 and 9). The possible eight phase domains are separated by phase boundaries, which intersect in two, three, or four quadrupole points. The complexity of the phase diagrams are explained with the effect of electrostatic interactions and binding of the counterions to the micelles. The largest micellar capacity of 0.448 is observed for C16-MES/C18-MES (60/40) in SLES-2EO and 0.354 for C16-MES/C18-MES (80/20) in AOS.

The new theoretical approach upgrades the available phase separation models in the literature [33–36]. The obtained maximal MES mole fraction of transparent micellar solutions could be of interest to increase the range of applicability of MES–surfactants in the presence of conventional anionic surfactants.

CRediT authorship contribution statement

Veronika I. Yavrukova: Data curation, Investigation. **Krassimir D. Danov:** Formal analysis, Software, Supervision, Writing – original draft, Writing – review & editing. **Tatiana G. Slavova:** Data curation, Investigation. **Rumyana D. Stanimirova:** Data curation, Investigation. **Yee Wei Ung:** Conceptualization, Funding acquisition, Project administration, Supervision. **Alvin Tong Kim Suan:** Data curation, Resources. **Hui Xu:** Data curation, Resources. **Jordan T. Petkov:** Conceptualization, Methodology.

Declaration of competing interest

The authors declare that they have no known competing financial interests or personal relationships that could have appeared to influence the work reported in this paper.

Data availability

Data will be made available on request.

Acknowledgements

The authors gratefully acknowledge the support from KLK OLEO. V.I. Yavrukova acknowledges the support from the National Program "Young scientist and postdoctoral students - 2" by the Bulgarian Ministry of Education and Science. K. Danov acknowledges the support from the Operational Programme "Science and Education for Smart Growth", Bulgaria, project No. BG05M2OP001-1.002-0023.

Appendix A. Supplementary data

Supplementary data to this article can be found online at https://doi.org/10.1016/j.jcis.2024.01.127.

References

[1] G.K.A. Parveez, E. Hishamuddin, S.K. Loh, M. Ong-Abdullah, K.M. Salleh, M.N.I.Z. Bidin, S. Sundram, Z.A.A. Hasan, Z. Idris, Oil palm economic performance in Malaysia and R&D progress in 2019, J. Oil Palm Res. 32 (2020) 159–190, 10.21894/jopr.2020.0032.

[2] S.Y. Low, J.Y. Tan, Z.H. Ban, P. Siwayanan, Performance of green surfactants in the formulation of heavy-duty laundry liquid detergents (HDLD) with special emphasis on palm based alpha methyl ester sulfonates (α-MES), J. Oleo Sci. 70 (2021) 1027–1037, https://doi.org/10.5650/jos.ess21078.

[3] Global Methyl Ester Sulfonate Market Outlook, Expert Market Research (EMR) Report, 2022, https://www.expertmarketresearch.com/reports/methyl-ester-sulfonate-market.

[4] N. Todori, T. Kakui, Methyl ester sulfonate, in: D.G. Hayes, D.K.Y. Salaiman, R. D. Ashby (Eds.), Biobased Surfactants. Synthesis, Properties, and Applications, 2nd edition,, Academic Press., Elsevier, 2019, pp. 303–324, https://doi.org/10.1016/C2016-0-03179-0.

[5] Z.A. Maurad, R. Ghazali, P. Siwayanan, Z. Ismail, S. Ahmad, Alpha-sulfonated methyl ester as an active ingredient in palm-based powder detergents, J. Surfactants Deterg. 9 (2006) 161–167, https://doi.org/10.1007/s11743-006-0386-7.

[6] D. Martinez, G. Orozco, S. Rincón, I. Gil, Simulation and pre-feasibility analysis of the production process of α-methyl ester sulfonates (α-MES), Bioresour. Technol. 101 (2010) 8762–8771, https://doi.org/10.1016/j.biortech.2010.06.059.

[7] H. Tulathammakit, B. Kitiyanan, Synthesis of methyl ester sulphonate surfactant from palm oil methyl ester by using UV or ozone as an initiator, Chem. Eng. Trans. 39 (2014) 421–426, https://doi.org/10.3303/CET1439071.

[8] Y. Jin, S. Tian, J. Guo, X. Ren, X. Li, S. Gao, Synthesis, characterization and exploratory application of anionic surfactant fatty acid methyl ester sulfonate from waste cooking oil, J. Surfactants Deterg. 19 (2016) 467–475, https://doi.org/10.1007/s11743-016-1813-z.

[9] J. Johansson, M. Svensson, Surfactant based on fatty acids and other natural hydrophobes, Curr. Opin. Colloid Interface Sci. 6 (2001) 178–188, https://doi.org/10.1016/S1359-0294(01)00076-0.

[10] R. Ghazali, Z.A. Maurad, P. Siwayanan, M. Yusof, S. Ahmad, Assessment of aquatic effects of palm-based alpha-sulfonated methyl ester (SME), J. Oil Palm. Res. 18 (2006) 225–230. http://jopr.mpob.gov.my/category/2001-2010/2006/vol-18-1-june-2006/.

[11] M. Luo, Z. Jia, H. Sun, L. Liao, Q. Wen, Rheological behavior and microstructure of an anionic surfactant micelle solution with pyroelectric nanoparticle, Colloids Surf. A 395 (2012) 267–275, https://doi.org/10.1016/j.colsurfa.2011.12.052.
[12] P. Siwayanan, R. Aziz, N.A. Bakar, H. Ya, R. Jokiman, S. Chelliapan, Detergency stability and particle characterization of phosphate-free spray dried detergent powders incorporated with palm C16 methyl ester sulfonate (C16MES), J. Oleo Sci. 63 (2014) 585–592, https://doi.org/10.5650/jos.ess13200.
[13] S. Itsadanont, J.F. Scamehorn, S. Soontravanich, D.A. Sabatini, S. Chavadej, Dissolution of soap scum by surfactant. Part I: effects of chelant and type of soap scum, J. Surfactants Deterg. 17 (2014) 849–857, https://doi.org/10.1007/s11743-013-1544-3.
[14] S. Itsadanont, P. Theptat, J.F. Scamehorn, S. Soontravanich, D.A. Sabatini, S. Chavadej, Dissolution of soap scum by surfactants. Part III. effect of chelant type on equilibrium solubility and dissolution rate of calcium and magnesium soap scums in various surfactant systems, J. Surfactants Deterg. 18 (2015) 925–932, https://doi.org/10.1007/s11743-015-1731-5.
[15] Y.S. Lim, R.D. Stanimirova, H. Xu, J.T. Petkov, Sulfonated methyl ester a promising surfactant for detergency in hard water conditions, H&PC Today 11 (2016) 47–51. https://www.teknoscienze.com/tks_issue/vol-114/.
[16] Y.S. Lim, N.B. Baharudin, Y.W. Ung, Methyl ester sulfonate: a high-performance surfactant capable of reducing builders dosage in detergents, J. Surfactants Deterg. 22 (2019) 549–558, https://doi.org/10.1002/jsde.12230.
[17] V.I. Yavrukova, G.M. Radulova, K.D. Danov, P.A. Kralchevsky, H. Xu, Y.W. Ung, J. T. Petkov, Rheology of mixed solutions of sulfonated methyl esters and betaine in relation to the growth of giant micelles and shampoo applications, Adv. Colloid Interface Sci. 275 (2020) 102062, https://doi.org/10.1016/j.cis.2019.102062.
[18] R.D. Stanimirova, P.A. Kralchevsky, K.D. Danov, H. Xu, Y.W. Ung, J.T. Petkov, Oil drop deposition on solid surfaces in mixed polymer-surfactant solutions in relation to hair- and skin-care applications, Colloids Surf. A 577 (2019) 53–61, https://doi.org/10.1016/j.colsurfa.2019.05.044.
[19] V.I. Yavrukova, D.N. Shandurkov, K.G. Marinova, P.A. Kralchevsky, Y.W. Ung, J. T. Petkov, Cleaning ability of mixed solutions of sulfonated fatty acid methyl esters, J. Surfactants Deterg. 23 (2020) 617–627, https://doi.org/10.1002/jsde.12393.
[20] R.L. Permadani, Slamet. Development of nanofluid detergent based on methyl ester sulfonates surfactant from waste cooking oil and titanium dioxide nanoparticles, IOP Conf. Ser.: Mater. Sci. Eng. 509 (2019) 012120, 10.1088/1757-899X/509/1/012120.
[21] X.-M. Tai, J.-Y. Song, Z.-P. Du, X. Liu, T. Wang, G. Wang, The performance test of fatty acid methyl ester sulfonates and application in the dishwashing liquid detergent, J. Dispers. Sci. Technol. 39 (2018) 1422–1426, https://doi.org/10.1080/01932691.2017.1409633.
[22] R.C. Soi, K.K. Pius, R. Kiplangat, Synthesis, characterization, and evaluation of solution properties of sesame fatty methyl ester sulfonate surfactant, ACS Omega. 5 (2020) 28643–28655, https://doi.org/10.1021/acsomega.0c03698.
[23] R. Ghazali, S. Ahmad, Biodegradability and ecotoxicity of palm stearin-based methyl ester sulfonates, J. Oil Palm. Res. 16 (2004) 39–44. http://jopr.mpob.gov.my/category/2001-2010/2004/vol-16-no-1-june-2004/.
[24] F. Abdullah, N.A.S. Ramli, F. Niikura, A.Z.A. Maurad, Physical properties of palm-based methyl ester sulfonate (MES) surfactant, Borneo Science, The Journal of Science and Technology 42 (2021) 34–47. http://borneoscience.ums.edu.my/?cat=78.
[25] K. Ohbu, M. Fujiwara, Y. Abe, Physicochemical properties of α-sulfonated fatty acid esters, Prog. Colloid Polym. Sci. 109 (1998) 85–92, https://doi.org/10.1007/BFb0118160.
[26] K.D. Danov, R.D. Stanimirova, P.A. Kralchevsky, E.S. Basheva, V.I. Ivanova, J. T. Petkov, Sulfonated methyl esters of fatty acids in aqueous solutions: interfacial and micellar properties, J. Colloid Interface Sci. 457 (2015) 307–318, https://doi.org/10.1016/j.jcis.2015.07.020.
[27] H. Xu, P. Li, K. Ma, R.J.L. Welbourn, J. Penfold, D.W. Roberts, R.K. Thomas, J. T. Petkov, Adsorption of methyl ester sulfonate at the air-water interface: can limitations in the application of the Gibbs equation be overcome by computer purification? Langmuir. 33 (38) (2017) 9944–9953, https://doi.org/10.1021/acs.langmuir.7b02725.
[28] H. Xu, R.K. Thomas, J. Penfold, P.X. Li, K. Ma, R.J.L. Welbourn, D.W. Roberts, J. T. Petkov, The impact of electrolyte on the adsorption of the anionic surfactant methyl ester sulfonate at the air-solution interface: Surface multilayer formation, J. Colloid Interface Sci. 512 (2018) 231–238, https://doi.org/10.1016/j.jcis.2017.10.064.
[29] H. Xu, P. Li, K. Ma, R.J.L. Welbourne, J. Doutch, J. Penfold, R.K. Thomas, D. W. Roberts, J.T. Petkov, K.L. Choo, S.Y. Khoo, Adsorption and self-assembly in methyl ester sulfonate surfactants, their eutectic mixtures and the role of electrolytes, J. Colloid Interface Sci. 516 (2018) 456–465, https://doi.org/10.1016/j.jcis.2018.01.086.
[30] E.S. Basheva, K.D. Danov, G.M. Radulova, P.A. Kralchevsky, H. Xu, Y.W. Ung, J. T. Petkov, Properties of the micelles of sulfonated methyl esters determined from the stepwise thinning of foam films and by rheological measurements, J. Colloid Interface Sci. 538 (2019) 660–670, https://doi.org/10.1016/j.jcis.2018.12.034.
[31] V.I. Ivanova, R.D. Stanimirova, K.D. Danov, P.A. Kralchevsky, J.T. Petkov, Sulfonated methyl esters, linear alkylbenzene sulfonates and their mixed solutions: micellization and effect of Ca2+ ions, Colloids Surf. A 519 (2017) 87–97, https://doi.org/10.1016/j.colsurfa.2016.06.039.
[32] F. Schambil, M.J. Schwuger, Physico-chemical properties of α-sulfo fatty acid methyl esters and α-sulfo fatty acid di-salts, Tenside Surf. Det. 27 (1990) 380–385, https://doi.org/10.1515/tsd-1990-270606.
[33] K.D. Danov, R.D. Stanimirova, P.A. Kralchevsky, T.G. Slavova, V.I. Yavrukova, Y. W. Ung, E. Tan, J.T. Petkov, Solubility of ionic surfactants below their Krafft point in mixed micellar solutions: phase diagrams for methyl ester sulfonates and nonionic cosurfactants, J. Colloid Interface Sci. 601 (2021) 474–485, https://doi.org/10.1016/j.jcis.2021.05.147.
[34] K.D. Danov, P.A. Kralchevsky, K.P. Ananthapadmanabhan, Micelle-monomer equilibria in solutions of ionic surfactants and in ionic-nonionic mixtures, Adv. Colloid Interface Sci. 206 (2014) 17–45, https://doi.org/10.1016/j.cis.2013.02.001.
[35] S.S. Tzocheva, P.A. Kralchevsky, K.D. Danov, G.S. Georgieva, A.J. Post, K. P. Ananthapadmanabhan, Solubility limits and phase diagrams for fatty acids in anionic (SLES) and zwitterionic (CAPB) micellar surfactant solutions, J. Colloid Interface Sci. 369 (2012) 274–286, https://doi.org/10.1016/j.jcis.2011.12.036.
[36] S.S. Tzocheva, K.D. Danov, P.A. Kralchevsky, G.S. Georgieva, A.J. Post, K. P. Ananthapadmanabhan, Solubility limits and phase diagrams for fatty alcohols in anionic (SLES) and zwitterionic (CAPB) micellar surfactant solutions, J. Colloid Interface Sci. 449 (2015) 46–61, https://doi.org/10.1016/j.jcis.2014.09.042.
[37] R. Farajzadeh, R. Krastev, P.L.J. Zitha, Foam films stabilized with alpha olefin sulfonate (AOS), Colloids Surf. A 324 (2008) 35–40, https://doi.org/10.1016/j.colsurfa.2008.03.024.
[38] D. Vollhardt, G. Czichocki, R. Rubert, Effect of the molecular structure on the adsorption of alkyl ether sulphates and alkane ether sulphonates at the air-water interface, Colloids Surf. A 142 (1998) 315–322, https://doi.org/10.1016/S0927-7757(98)00356-2.
[39] J. Lucassen, Hydrolysis and precipitates in carboxylate soap solutions, J. Phys. Chem. 70 (1966) 1824–1830, https://doi.org/10.1021/j100878a022.
[40] P.A. Kralchevsky, K.D. Danov, C.I. Pishmanova, S.D. Kralchevska, N.C. Christov, K. P. Ananthapadmanabhan, A. Lips, Effect of the precipitation of neutral-soap, acid-soap, and alkanoic acid crystallites on the bulk pH and surface tension of soap solutions, Langmuir. 23 (2007) 3538–3553, https://doi.org/10.1021/la0625401.
[41] D.J. Mitchell, B.W. Ninham, Electrostatic curvature contributions to interfacial tension of micellar and microemulsion phases, J. Phys. Chem. 87 (1983) 2996–2998, https://doi.org/10.1021/j100239a003.
[42] P.A. Kralchevsky, K.D. Danov, G. Broze, A. Mehreteab, Thermodynamics of ionic surfactant adsorption with account for the counterion binding: effect of salts of various valency, Langmuir. 15 (1999) 2351–2365, https://doi.org/10.1021/la981127t.
[43] P.A. Kralchevsky, K.D. Danov, V.L. Kolev, G. Broze, A. Mehreteab, Effect of nonionic admixtures on the adsorption of ionic surfactants at fluid interfaces: 1, Sodium Dodecyl Sulfate and Dodecanol, Langmuir. 19 (2003) 5004–5018, https://doi.org/10.1021/la0268496.
[44] K.D. Danov, P.A. Kralchevsky, S.D. Stoyanov, J.L. Cook, I.P. Stoot, Analytical modeling of micelle growth. 3. electrostatic free energy of ionic wormlike micelles – effects of activity coefficients and spatially confined electric double layers, J. Colloid Interface Sci. 581 (2021) 262–275, https://doi.org/10.1016/j.jcis.2020.07.059.
[45] D.N. Rubingh, Mixed micelle solutions, in: K.L. Mittal (Ed.), Solution Chemistry of Surfactants, Vol. 1, Springer, Boston, MA, 1979, pp. 337–354, https://doi.org/10.1007/978-1-4615-7880-2_15.
[46] R. Nagarajan, E. Ruckenstein, Theory of surfactant self-assembly: a predictive molecular thermodynamic approach, Langmuir. 7 (1991) 2934–2969, https://doi.org/10.1021/la00060a012.
[47] H.W. Stache (Ed.), Anionic Surfactants: Organic Chemistry, 1st edition, CRC Press, 1995.